Downscaling CESM2 in CLM5 to Hindcast Pre-Industrial Equilibrium Line Altitudes for Tropical Mountain Glaciers

Nicholas G. Heavens[1,2]

[1]Space Science Institute, 4765 Walnut St, Suite B, Boulder, CO 80301, USA
[2]Department of Earth Science and Engineering, Imperial College, London, United Kingdom

Key Points:

- Global model-forced standalone land model framework developed for simulating tropical mountain glaciation
- Equilibrium line altitude can be estimated with a bias of 237 ± 340 m where mountain peaks sufficiently resolved
- Uncertainties in mean lapse rate of temperature or downwelling longwave radiation are minor or irrelevant contributors to bias

Corresponding author: Nicholas G. Heavens, nheavens@spacescience.org

Abstract

Tropical mountain glaciers are an important water resource and highly impacted by recent climate change. Tropical mountain glaciation also occurred in the deep past, raising questions about their global climate significance and presenting challenges for bridging the scales resolved by global models (100s of km) with the $\approx$ 1–10 km scale of glaciers when paleotopography is poorly known. Here we hindcast tropical mountain glaciation in pre-industrial time by using global climate model meteorology to force standalone simulations in its land component that use high resolution topography to resolve selected tropical mountain glaciers. These simulations underestimate observed equilibrium line altitudes (ELA) by 237 $\pm$ 340 m, but the simulated ELA and snow lines capture observed inter-mountain ELA variability. Uncertainties in flow and temperature/downward longwave radiation lapse rates do not fully explain ELA hindcast bias, suggesting diurnal variability not captured by downscaling may be an important bias factor.

Plain Language Summary

Shrinking glaciers in mountains near the Equator are commonly used to illustrate present day climate change caused by greenhouse gas emissions from burning fossil fuels. These glaciers are not just picturesque but also can be an important source of water for humans. Geologists have found the traces of larger, lower elevation glaciers from the most recent ice age and hundreds of millions of years ago. These glaciers could be big clues to how cold climate was in the past, if we knew how to interpret them. Climate models could help, but they generally look at what is happening at scales much bigger than glaciers. We would like to be able to predict how low glaciers reach in elevation in a particular global climate model experiment. We do this by taking the weather from a global climate model and putting into a model that looks at processes similar in scale to glaciers. This approach underestimated the elevation of several well-observed glaciers, even if we accounted for glaciers flowing and other potential problems in translating information from the global to glacier scale. But our method does get right how glacier elevation varies from mountain to mountain, which is potentially useful.

1 Introduction

Mountain glaciers in the Earth's tropics can be a striking part of the landscape, because their high reflectivity at all visible wavelengths and their very nature as frozen water can starkly contrast with the red, brown, and green colors and warmer and/or drier climates at nearby lower elevations. The shrinking of tropical mountain glaciers over the last century or so has been used as a potent illustration of the impact of anthropogenic climate change on an aesthetically compelling feature of the environment (e.g., Mote & Kaser, 2007; Thompson et al., 2011). But the shrinking of these glaciers has more practical consequences for those who depend on them for fresh water or other climate services, principally in the Andes (e.g., Vuille et al., 2008; Mölg et al., 2008; Drenkhan et al., 2015)

Tropical mountain glaciers make such a good and potentially misleading (see Mote & Kaser, 2007) illustration of anthropogenic climate change, because they are highly sensitive to changes in temperature and precipitation. The equilibrium line altitude (ELA), the elevation at which long-term accumulation of ice balances long-term ablation of ice, was typically $\approx$ 1 km lower at the Last Glacial Maximum (LGM) than the period around or just after 1850 (Porter, 2001; Hastenrath, 2009). This change was coincident with a 2–4 K change in tropical mean temperatures (Annan & Hargreaves, 2013), which was likely larger on mountains due to steeper lapse rates (Tripati et al., 2014; Loomis et al., 2017).

It is important to note that the ELA is a global property of a glacier. In areas with steeper slopes, glaciers can flow quite deeply into valleys, emplacing terminal moraines at elevations $>$ 1 km below the ELA that is rigorously obtained by taking of the mean elevation of the entire margin of the glacial front (Osmaston, 2004) and less rigorously by averaging the top and bottom elevation of the glacier (Porter, 2001).

Global climate at the LGM was relatively cold for Phanerozoic time and highland environments are preferentially eroded (Larsen et al., 2014; Mills et al., 2021), so evidence for tropical mountain glaciation would not be expected to be widespread in the geologic record. As early as the nineteenth century, however, past glaciation was recognized in a highland environment adjacent to tropical lowlands dating from the Late Carboniferous Period of France (300 Ma) (Julien, 1895). Modern techniques have confirmed the Late Carboniferous age and paleolatitude of glacial deposits from France as well as in an ancient tropical mountain range far to the west in present day Colorado (e.g., Soreghan et al., 2014; Pfeifer et al., 2021, and references therein). These Carboniferous deposits seem to record terminal moraines at altitudes $<$ 2000 m, suggesting ELA was at least similar to the LGM (Soreghan et al., 2014). However, global climate model (GCM) simulations using appropriate paleogeography and plausible greenhouse gas levels have been unable to reproduce stable glaciation at these elevations (Soreghan et al., 2008; Heavens et al., 2015).

A GCM might be unable reproduce past glaciation if it is under-resolving or incompletely representing glacial processes. Typical GCM resolution for lengthy deep time climate experiments are 200–400 km at the Equator (Soreghan et al., 2008; Heavens et al., 2015), while even pre-industrial tropical glaciers typically were $<<$ 10 km in diameter (Kaser, 1999). And while deep time GCMs generally predict snowfall and some work has been done to couple deep time GCMs with models that simulate ice sheets (e.g., Hyde et al., 2000; Poulsen et al., 2007; Horton et al., 2012), prognostic climate simulations of mountain glaciation are relatively rare and require some form of downscaling from global GCM resolution (e.g., Kotlarski et al., 2010; Shannon et al., 2019).

Recently, a prognostic ice sheet model, the Community Ice System Model (CISM), was added as a fully coupled component to the Community Earth System Model (Lipscomb et al., 2019). CISM takes ice mass balance information from the Community Land Model (CLM), which CLM predicts on the basis of atmospheric component (Community Atmosphere Model: CAM) temperature and precipitation information downscaled into multiple elevation classes of potential glaciers. Thus, the ice mass balance a large grid cell is considered at an elevation around 3000 m, 2500 m, etc. according to model settings. CISM then translates that ice mass balance onto a grid with resolution as fine as 4 km and simulates ice flow. But CLM (with or without CISM) is not designed to simulate mountain glaciation realistically because of concerns that under-resolving topography within the atmosphere model results in excessively warm climate and excessive runoff (UCAR, n.d.).

The purpose of this study is to use CESM and CLM when topography is explicitly resolved to predict the ELA of tropical mountain glaciation in a limited area and test these predictions against observations. This hindcasting framework uses CLM forced by CAM to obtain ice surface mass balance (SMB) information but downscales atmospheric forcing to a high resolution topographic grid. Trying to connect global climate change quantitatively with the response of tropical mountain glaciation is nothing new (see Mölg and Kaser (2011); Roe et al. (2021) and references therein). The unique feature of this study is modeling tropical mountain glaciation entirely within the framework of a latest generation global climate model and its land component. While this hindcasting framework is being developed for deep time climate studies, the validation test that it provides for CESM2 and CLM5 and could provide for global climate models of similar capability should be of broader interest.

2 Methods

2.1 CESM2 and CLM Simulations

We performed standalone CLM5 simulations forced by a data atmosphere generated by a standard CESM2 simulation on the National Center for Atmospheric Research (NCAR) supercomputer Cheyenne (CISL, 2019). Because this is a non-standard configuration of CLM5, we have archived example case directories, configuration procedure documentation, and input files for these simulations within the data archive associated with this study (Heavens, 2021). CESM2 and CLM5 (its default land component) were particularly chosen, because CLM5 was specifically modified to improve representation of processes related to hydrology, snowfall, and ice mass balance (Lawrence et al., 2019). Except for some simulations described later, the CLM5 code was modified to remove a step in the downscaling of downward longwave radiation at the surface (FLDS) that renormalized the downscaled radiation fields between elevation classes. This change is consistent with each point in the land model being treated as a single elevation class and reduces FLDS on mountain summits by $\approx$ 100 Wm^{-2}.

The CESM2 data atmosphere came from 30 years of a branch simulation from year 1101 of the Climate Model Intercomparison Project 6 (CMIP6) standard pre-industrial control for CESM2 at f09_g17 resolution (0.9° × 1.25°) (Danabasoglu et al., 2020). Standalone CLM5 simulations then were run in 10 limited area domains roughly centered on past or presently glaciated tropical mountains with well-documented estimates of ELA (Table 1). Two areas with no recently glaciated mountains but with mountains that were glaciated at the LGM (Table 1) were simulated to make sure ELA was not substantially underestimated in pre-industrial climate and to set a baseline for a future study of LGM tropical mountain glaciation. The selected areas cover a meridional transect in the tropics of Central and South America as well as a few domains in Africa and the Maritime Continent to cover a range of observed ELA and proximity to the ocean. This choice of domains is meant to span the potential range of precipitation, though this choice cannot be rigorous because of the sparseness of precipitation measurements and the heteorogeneity of precipitation in these areas (e.g., La Frenierre & Mark, 2017).

Each domain was 2° in latitude and 1° in longitude. The selection of domain size ensured multiple glaciated mountains and topography < 2000 m could be included in the domain (except in the High Andes). The domain is similar in size to 1–2 global model grid cells in the CESM2 simulation.

Each CLM5 simulation was initialized from high-resolution surface data and land domain files (nominally 100 points per degree) in which the global model resolution land surface properties except topography/slope were translated to the high-resolution domain by nearest neighbor interpolation. High resolution topography, standard deviation of elevation, and slope data were then added using 30 arc-second resolution data from GMTED2010 (Danielson & Gesch, n.d.). (Fig. 1a). The topography was used to assign each grid point to one of 10 possible elevation classes and set its elevation. To ensure SMB could be calculated, glacial column coverage was set to a minimum of 1% (or greater where the original land surface dataset had greater glacial column coverage). This additional glacial column coverage replaced coverage by vegetation. Glacier region was set to 2 (Greenland). We have verified by appropriate simulations that using the different elevation class treatments available for glacier regions 2 and 3 (Antarctica) or using 50% glacial coverage does not affect the results of this type of simulation as long as the SMB and related calculations are analyzed on the glaciated land units alone. In effect, these experiments impose a glacier of 50 m altitude (as evident from the documentation and initial grid cell ice content variable, ICE_CONTENT1) over a limited grid cell area, in circumstances where glaciation has no or minimal impact on large-scale climate, and simulate how it accumulates or ablates over a climatological normal period.

[]

Table 1. High resolution domains used for standalone CLM5 simulations. Features listed and ELA values come from Porter (2001) and Hastenrath (2009). Distance from the ocean was calculated using the distance calculator in Google Earth and is listed with a 5 km precision.

Number	**Latitude Bounds (°N)**	**Longitude Bounds (°E)**	**Mountains/ Features**	**Est. Pre-Industrial ELA (m)**	**Minimum Distance from Ocean (km)**
1	18.5, 20.5	-99.5, -98.5	Iztaccihuatl, Mexico	4880	225
2	8.5, 10.5	-84,-83	Cherro Chirripo, Costa Rica	>3819	50
3	4,6	-76,-75	Los Nevados de Santa Isabel y del Ruiz, Colombia	4750, 4850	220, 235
4	-2, 0	-79,-78	Chimborazo+ Antisana, Ecuador	4715, 4850	210, 215
5	-10,-8	-78,-77	Huascaran, Peru	5000	95
6	-18.5,-16.5	-69.85,-68.85	Nevado Sajama, Bolivia; Parinacota, Chile	5550, 5600	160, 115
7	-1,1	37,38	Mt. Kenya, Kenya	4712.5	440
8	-4,-2	37,38	Mt. Kilimanjaro, Tanzania (Kibo and Mawenzi peaks)	5030, 5407.5	285
9	-1,1	29.5,30.5	Mt. Ngaliema, Uganda	4495	1205
10	5,7	116,117	Kinabalu, Malaysia	>4095	40

The experiments were cold started (because only physical climate was of interest) and used crop-biogeochemistry physics routines, because agricultural activity occurs in some of the domains and it was therefore necessary to include crop biomes. Lapse rate was set to the mean free air temperature lapse rate for the domain derived from the CESM2 simulation. FLDS lapse rate was set to the standard CLM5 setting of 0.032 $\mathrm{W m^{-2}\ m^{-1}}$ Van Tricht et al. (2016); Lawrence et al. (2019). (Positive lapse rate is defined here as decreasing with height.)

The mean free air lapse rate in each CLM5 domain was calculated by calculating the mean lapse rate in the troposphere as defined by WMO (1957) for every grid point of each monthly mean output file of the CESM2 simulation, interpolating this onto each CLM5 domain in the same way as the CLM5 boundary condition files, and then averaging over 30 years. The results in all cases are between 6 and 7 K $\mathrm{km^{-1}}$ (Table 2).

To test sensitivity to FLDS and temperature lapse rate, six simulations were performed in domain 4 (Table 1) that varied temperature lapse rate in six steps (9.8, 8, 7, 6, 5, 3.2 K $\mathrm{km^{-1}}$) without modifying the FLDS downscaling in CLM5. These values span the dry adiabatic lapse rate and extreme values reported by Shen et al. (2016) for the mid-latitude Tianshan Mountains. An additional simulation in domain 4 was performed with the FLDS downscaling modified and a temperature lapse rate of 7 K $\mathrm{km^{-1}}$.

2.2 Analysis

The results of each simulation then were analyzed to extract ELA and ELA-related metrics. ELA, strictly speaking, is the elevation where ablation and accumulation are in balance, that is, where long-term SMB is equal to zero. Following Vizcaíno et al. (2014),

$$SMB = SNOW + RAIN - RUNOFF - SUBLIMATION \tag{1}$$

This balance can be expressed in CLM5 output variables restricted to glaciated land units only.

$$SMB = SNOW\_ICE + RAIN\_ICE - QRUNOFF\_ICE - QFLX\_SUB\_SNOW\_ICE \tag{2}$$

where the quantities in brackets correspond to the terms of Eq. 1 and SNOW_ICE, RAIN_ICE, QRUNOFF_ICE, and QFLX_SUB_SNOW_ICE are variables output by CLM5. From this point onward, we will use SMB to mean the integrated SMB over the 30 year period of each simulation (Fig. 1b).

ELA in the absence of flow (ELA$_{noflow}$) was estimated by dividing the domain into connected regions with SMB $>$ 0. ELA then was defined as the minimum altitude of each region. By determining the maximum altitude of each region, it was possible to assign each region to a mountain with observed ELA estimates. In some cases, however, two mountain peaks with estimates were in the same connected region.

An ELA metric accounting for flow (ELA$_{flow}$) was calculated by first estimating the minimum possible elevation of a terminal moraine originating from each connected regions with SMB > 0. The product of SMB and area for each connected region as well as the path with steepest slope connected to the maximum altitude of the region were determined. The product of SMB and area in the ablation region along this path were integrated and subtracted from the sum of SMB and area in the accumulation zone formed by the connected regions. This is equivalent to determining how low in elevation could the accumulated ice go if ice were continuously delivered along a one grid cell wide valley originating from the region. ELA$_{flow}$ then was estimated as the average of the peak

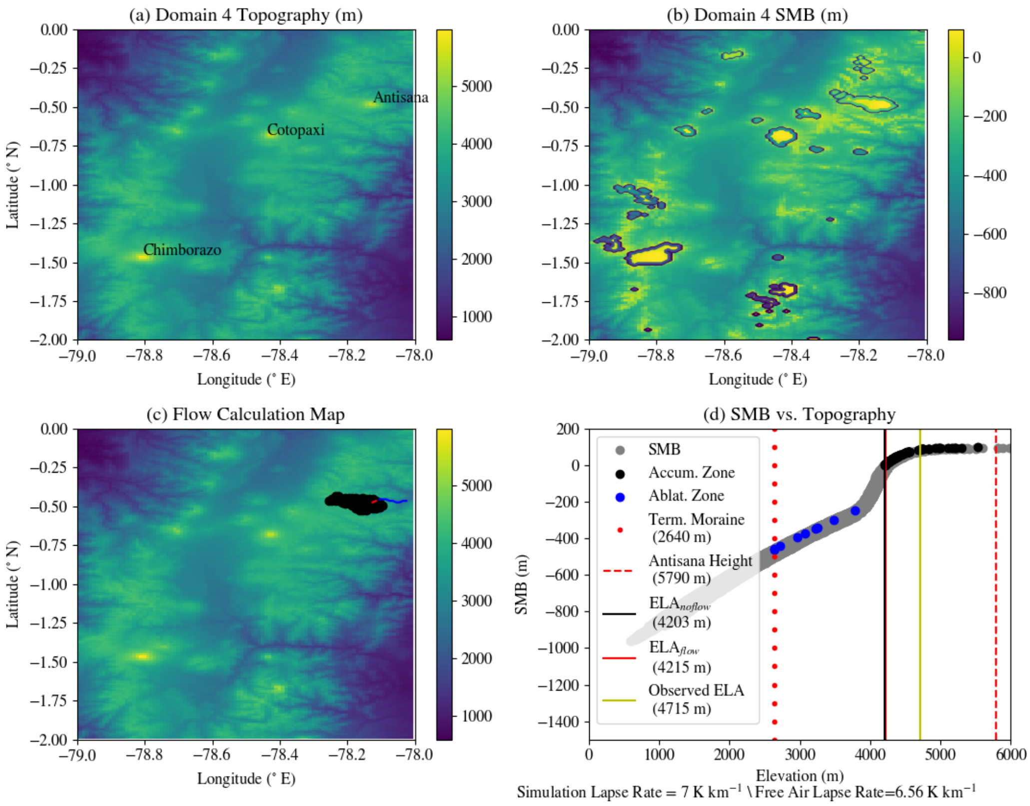

Figure 1. Example CLM5 standalone simulation and its analysis, as labeled: (a) Topographic grid (m). Mountains of interest are labeled, but only Chimborazo and Antisana have ELA estimates; (b) Net SMB for the simulation (m). Connected regions (accumulation zones) are indicated by contours; (c) Topographic map (m) showing the accumulation zone for Antisana in black and the steepest path from the peak used to find the minimum elevation for a terminal moraine in blue; (d) SMB vs. topography for the entire domain with relevant estimates and observations for Antisana labeled.

altitude of the region and the elevation of the terminal moraine in line with a typical technique for estimating ELA in the field (Porter, 2001). This type of calculation is illustrated in Figs. 1c–d.

The snow line has been used to approximate ELA under some circumstances (Porter, 2001). So for comparison, two estimates of the permanent snow line also were calculated. SL and SL_{1m} were defined as the minimum altitude at which snow and snow of 1 m depth were present in each month during the last month of the simulation, respectively. These metrics were calculated for the whole domain by averaging the minimum elevation where snow is present and the maximum elevation where snow is absent by analogy with the glaciation-threshold method (Porter, 2001). In each case, snow depth was normalized by the fraction of glacial coverage to obtain the true snow depth in the glacial column. Note that SL_{1m} tends to highlight a small range of elevation where snow depth rapidly increases: a true snow line. Thus, choosing a much higher depth criterion only would marginally change ELA. In one simulation, SL_{1m} is 4362 m, but SL_{10m} is only 4405 m.

3 Results

The results of this analysis are given in Table 2. The non-glaciated mountains of Ajusco, Cerro Chrirripo, and Kinabulu all are hindcast as non-glaciated. However, the simulations also hindcast Mts. Kenya and Ngaliema as being non-glaciated. This is most likely a resolution problem. For Mt. Ngaliema, uncertainty in the observed ELA is large and the upper bound of ELA it implies is greater than the height of Mt. Ngaliema resolved by the model (Table 2). For Mt. Kenya, the observed ELA is within 100 m of the model-resolved height (Table 2). The model domains do not resolve the highest peaks in several other cases, but the highest elevation in the model is typically significantly greater than the ELA. A similar resolution problem makes it difficult to resolve Kibo from Mawenzi peaks on Kilimanjaro, so Kibo peak only will be considered in the remainder of the analysis.

For nine sufficiently resolved mountains with observed glaciation, the bias (Δ) in the simulated ELA for each of the metrics was estimated by taking the mean and standard deviation of the difference between the estimated and observed ELA (Fig. 2). ELA_{noflow} underestimates observed ELA by 237 $\pm$ 340 m. Accounting for flow (ELA_{flow}) reduces the underestimate to 120 m but widens the uncertainty. But as noted by (Porter, 2001), the method used to derive ELA from terminal moraine elevation may overestimate ELA by up to 150 m, making ELA_{flow} no superior to that derived based on SMB alone. The average simulated snow line is 1084 m below the observed ELA. However, requiring 1 m of permanent snow depth reduces this underestimate to 318 m with comparable uncertainty to ELA, suggesting that the snow line illustrated in Fig. S1 is a good approximation to ELA rather than a snow line based on a minimal amount of snow. The magnitude and variability of biases in all ELA metrics are large enough that they exceed the largest reported uncertainties in observed ELA.

The simulated ELA metrics follow the variability in observed ELA (Fig. 2). Higher observed ELA usually results in higher simulated ELA, suggesting that the simulated ELA is capturing the variability in observed ELA but underestimating its magnitude. For example, the correlation between ELA_{noflow} and SL_{1m} and observed ELA is 0.92 and 0.93 respectively (n=9), which is significant to $p<0.001$. This correlation is weaker for the other metrics but is still significant to $p<0.05$.

Possible sources of error are the major free parameters of the experiments, the lapse rates of temperature and FLDS, particularly in domain 4. We first consider temperature lapse rate. In domain 4, ELA is underestimated by $\sim$ 400 m (Fig. 2. As implied by the relevant simulation in Table 2, increasing the lapse rate by 1 K lowers ELA_{noflow} by 330 m. So if the free air lapse rate were considerably higher than the near-surface lapse rate over high terrain, this effect could explain the bias. However, Córdova et al. (2016) used weather station data over the Ecuadorian Andes ($\sim$ 50 km south of domain 4 of Table 2) to show that mean lapse rate was 6.9 K km^{-1}, 0.3 K km^{-1} greater than that of domain 4 and thus in the opposite direction necessary to explain the bias. It is unlikely that the lapse rate would decrease at elevations greater than the 4200 m elevation of the highest weather stations sampled by Córdova et al. (2016).

Despite being derived from observations over Greenland (Van Tricht et al., 2016), the lapse rate in FLDS also agrees well with available observations in domain 4. Wagnon et al. (2009) measured annual mean FLDS on Antisana to be 283 Wm^{-2} during 2005–2006. We used the assumed lapse rate in FLDS to translate between the elevation of these observations and the elevation of the nearest grid point in the high resolution grid ($\sim$ 300 m). We then compared the annual mean FLDS at the nearest grid point in the CESM2 simulation with the annual mean FLDS for the period sampled by Wagnon et al. (2009) in the CESM2 CMIP6 historical simulation (b.e21.BHIST.f09_g17.CMIP6-historical.003) at the same grid point. This comparison implies FLDS was 1.4 Wm^{-2} greater during 2005–2006 than around 1850. With all of these adjustments made, the expected annual

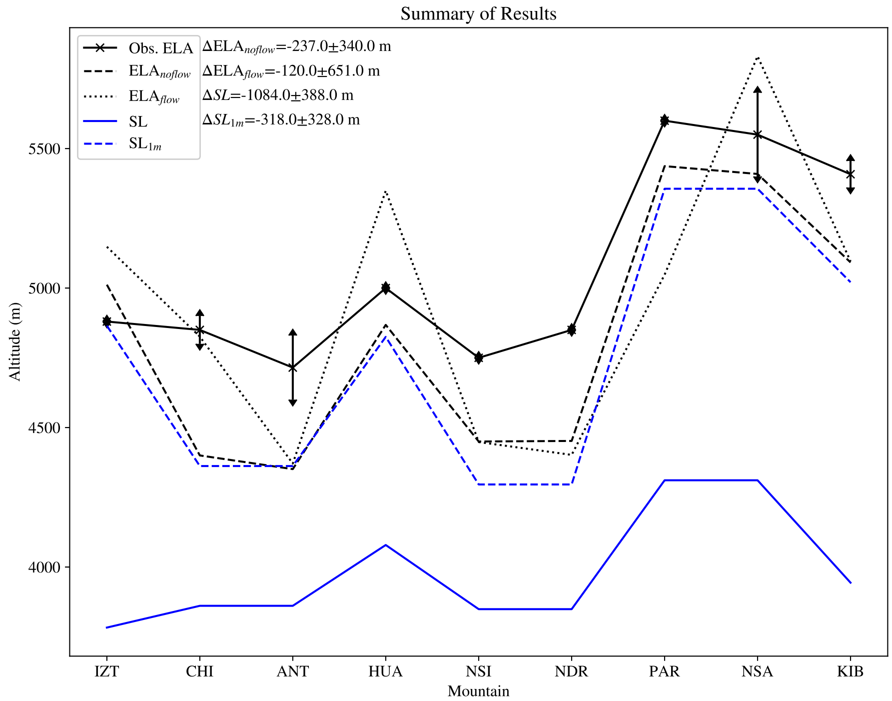

Figure 2. Comparison of different ELA estimates with observed ELA and their uncertainties for mountains with both observed and simulated ELA. Abbreviated mountain names on the x-axis are abbreviated and in the same order as Table 2. The estimated mean bias and 2σ uncertainty in each metric is listed next to the legend.

mean FLDS in standalone CLM5 simulations at Wagnon et al. (2009)'s observation site on Antisana should be 275 Wm^{-2}, 8 Wm^{-2} lower than observed. This is equivalent to a +8% error in the assumed FLDS lapse rate. If the standard CLM5 downscaling is used, the annual mean FLDS is 381.41 Wm^{-2}. At a temperature lapse rate of 7 K km^{-1}, the sensitivity in ELA$_{noflow}$ to FLDS is 9.2 m (Wm^{-2})$^{-1}$, so this would explain an ELA$_{noflow}$ underestimate of 77 m, 21% of ΔELA$_{noflow}$ at Antisana. (Interpolating the results of the standard CLM5 downscaling simulations to 6.56 K km^{-1} and differencing with the 6.56 K km^{-1} lapse rate modified downscaling simulation for domain 4 only changes this result to 87 m and 24%).

4 Discussion

Whether ELA is based on SMB or permanent snow cover, our CESM2–CLM5 framework significantly underestimates ELA, implying a cold bias in simulating tropical mountain climates in these models. This result is somewhat surprising in light of the concern expressed in UCAR (n.d.) that using CLM5 to study mountain glaciation would be impacted by a warm bias. On average, accounting for ice flow enhances the discrepancy between simulated and observed ELA, implying neglecting flow is not a major source of error. Nor do the lapse rate settings of the simulations seem to explain the bias between hindcast and observed ELA. Moreover, while the high resolution grid does not perfectly resolve mountain peaks and likely under-resolves the potentially smaller African glaciers

[]

Table 2. Results of the CLM5 standalone simulations for each mountain of interest. Ice-free and snow-free indicate where glaciation is not observed or ELA cannot be defined, MWHP indicates merger of glaciation of that mountain with a higher peak. Italicized mountain names indicate simulations and moountains used to estimate bias in simulated ELA. ELA data come from Porter (2001) and Hastenrath (2009)

Mountain	**Domain Lapse Rate (K/km)**	**Longwave Downscaling**	**Height (m)**	**Height in Model (m)**	**Obs. ELA (m)**	**ELA**$_{noflow}$ **(m)**	**ELA**$_{flow}$ **(m)**	**SL (m)**	**SL**$_{1m}$ **(m)**
Iztaccihuatl	6.39	Modified	5286	5012	4880	5012	5148	3783	4865
Ajusco	6.39	Modified	3937	3720	Ice-free	Ice-free	Ice-free	3826	Snow-free
Cerro Chirripo	6.45	Modified	3819	3656	Ice-free	Ice-free	Ice-free	Snow-free	Snow-free
Chimborazo	6.56	Modified	6310	5983	4850±50	4400	4826	3861	4362
Chimborazo	9.8	CLM5 Standard	6310	5983	4850±50	4048	4826	3270	4013
Chimborazo	8	CLM5 Standard	6310	5983	4850±50	4656	5035	3672	4588
Chimborazo	7	CLM5 Standard	6310	5983	4850±50	5072	5356	3971	5039
Chimborazo	6	CLM5 Standard	6310	5983	4850±50	5811	5905	4379	5703
Chimborazo	5	CLM5 Standard	6310	5983	4850±50	Ice-free	Ice-free	4959	Snow-free
Chimborazo	3.2	CLM5 Standard	6310	5983	4850±50	Ice-free	Ice-free	Snow-free	Snow-free
Chimborazo	7	Modified	6310	5983	4850±50	4255	4826	3729	4217
Antisana	6.56	Modified	5790	5529	4715±115	4351	4371	3861	4362
Antisana	9.8	CLM5 Standard	5790	5529	4715±115	MWHP	MWHP	3270	4013
Antisana	8	CLM5 Standard	5790	5529	4715±115	4552	4694	3672	4588
Antisana	7	CLM5 Standard	5790	5529	4715±115	5105	5191	3971	5039
Antisana	6	CLM5 Standard	5790	5529	4715±115	Ice-free	Ice-free	4379	5703
Antisana	5	CLM5 Standard	5790	5529	4715±115	Ice-free	Ice-free	4959	Snow-free
Antisana	3.2	CLM5 Standard	5790	5529	4715±115	Ice-free	Ice-free	Snow-free	Snow-free
Antisana	7	Modified	5790	5529	4715±115	4203	4215	3729	4217
Huascaran	6.65	Modified	6768	6293	5000	4868	5349	4079	4825
Nevado de Santa Isabel	6.56	Modified	4950	4814	4750	4450	4448	3849	4296
Nevado del Ruiz	6.56	Modified	5321	5215	4850	4452	4402	3849	4296
Parinacota	6.8	Modified	6348	6240	5600	5437	5048	4311	5356
Nevado Sajama	6.8	Modified	6542	6240	5550±150	5409	5831	4311	5356
Mt. Ngaliema	6.59	Modified	5109	4670	4495±225	Ice-free	Ice-free	3812	Snow-free
Mt. Kenya	6.54	Modified	5202	4839	4712.5±12.5	Ice-free	Ice-free	4023	Snow-free
Mawenzi (Kilimanjaro)	6.45	Modified	5147	blends with Kibo	5030	MWHP	MWHP	3944	5021
Kibo (Kilimanjaro)	6.45	Modified	5895	5794	5408±47.5	5092	5096	3944	5021
Kinabulu	6.66	Modified	4095	3985	Ice-free	Ice-free	Ice-free	3897	Snow-free

(areas on the order of 1 km^2, Andean glacier areas are on the order of 10 km^2 in area and should be resolved (Kaser, 1999).

A possible source of error that cannot be easily evaluated is diurnal and spatial variability in lapse rate at the topographic scale. Córdova et al. (2016) observed lapse rates in maximum temperatures of 8.8 K km^{-1} and 5.5 K km^{-1} in minimum temperatures. Studied of lapse rates over the mountainous regions in the mid-latitudes likewise sugggest that the atmospheric lapse rate can be a poor approximation for the decrease in surface temperature and the near-surface air temperature with elevation because of preferential solar heating of slopes, drainage of cold air into valleys, and variations in surface cover by snow or vegetation (Minder et al., 2010; Pepin et al., 2016). Thus, failure of CLM5 to account for diurnal variability or properly represent drainage flows or asymmetry in surface heating might result in excessive melting and substantially raise the simulated ELA. Adjusting our hindcasting framework to account for this variability likely would require an embedded mesoscale atmospheric model, raising computational cost and further limiting our ability to apply this framework to other global climate states where 1 km scale topography is unknown.

There is a positive note for using this hindcasting framework for investigating past tropical mountain glaciation in other climate states. ELA based on SMB or substantial surface snow cover captures the variability in observed ELA. Thus, if the ELA bias is just an offset caused by insufficiently considering local thermal structure in the downscaling or some other model bias, it still may be possible to hindcast the rise or fall in ELA with different global climate states by testing against an ensemble of mountains like those compiled for this study. It thus would be appropriate to repeat this study for LGM conditions and see if the observed depression in ELA between the LGM and pre-industrial climate is reproduced.

5 Summary

In this study, we have tested downscaling CESM2 global simulations in CLM5 to hindcast tropical mountain glaciation. Our eventual objective for developing this hindcasting framework is to interpret the significance of deep past tropical mountain glaciation for global climates. But this technique may be more broadly valuable for model validation for models analogous in capability to CESM2 and CLM5. While our framework well captures the variability in glaciation between different tropical mountains, it generally underestimates glacier ELA by a larger margin than the uncertainty in the observations. However, this bias is still smaller than the 1 km difference between ELA during the LGM and pre-industrial time, suggesting that this framework might accurately capture the change in ELA between different global climate states. This hypothesis could be verified by repeating this study for LGM conditions. Moreover, making ELA estimates based on snow line rather than surface mass balance looks promising for simulating ELA in circumstances where topography is poorly known.

Acknowledgments

Supporting datasets and analytical code for this research are available in Heavens (2021). The CMIP6 CESM2 historical simulation is available in NCAR (2018). This work was funded by the Sedimentary Geology and Paleobiology program of the National Science Foundation (EAR-1849754).

References

Annan, J. D., & Hargreaves, J. C. (2013). A new global reconstruction of temperature changes at the last glacial maximum. *Climate of the Past*, *9*(1), 367–376. Retrieved from https://cp.copernicus.org/articles/9/367/2013/ doi: 10

.5194/cp-9-367-2013

CISL. (2019). *Cheyenne: HPE/SGI ICE XA System (University Community Computing).* Boulder, CO: National Center for Atmospheric Research. doi: 10.5065/D6RX99HX

Córdova, M., Célleri, R., Shellito, C. J., Orellana-Alvear, J., Abril, A., & Carrillo-Rojas, G. (2016). Near-Surface Air Temperature Lapse Rate Over Complex Terrain in the Southern Ecuadorian Andes: Implications for Temperature Mapping. *Arctic, Antarctic, and Alpine Research*, *48*(4), 673-684. Retrieved from https://doi.org/10.1657/AAAR0015-077 doi: 10.1657/AAAR0015-077

Danabasoglu, G., Lamarque, J.-F., Bacmeister, J., Bailey, D. A., DuVivier, A. K., Edwards, J., ... Strand, W. G. (2020). The Community Earth System Model Version 2 (CESM2). *Journal of Advances in Modeling Earth Systems*, *12*(2), e2019MS001916. Retrieved from https://agupubs.onlinelibrary.wiley.com/doi/abs/10.1029/2019MS001916 (e2019MS001916 2019MS001916) doi: https://doi.org/10.1029/2019MS001916

Danielson, J., & Gesch, D. (n.d.). *Global multi-resolution terrain elevation data 2010 (GMTED2010)* (No. 2011–1073). USGS Open File Report.

Drenkhan, F., Carey, M., Huggel, C., Seidel, J., & Oré, M. T. (2015). The changing water cycle: climatic and socioeconomic drivers of water-related changes in the Andes of Peru. *WIREs Water*, *2*(6), 715-733. Retrieved from https://onlinelibrary.wiley.com/doi/abs/10.1002/wat2.1105 doi: https://doi.org/10.1002/wat2.1105

Hastenrath, S. (2009). Past glaciation in the tropics. *Quaternary Science Reviews*, *28*(9), 790-798. Retrieved from https://www.sciencedirect.com/science/article/pii/S0277379108003521 doi: https://doi.org/10.1016/j.quascirev.2008.12.004

Heavens, N. G. (2021). *CESM2-CLM5 Framework for Hindcasting Tropical Mountain Glaciation: Examples and Pre-Industrial Validation Analysis.* Mendeley Data. doi: 10.17632/68cdfyssgs.1

Heavens, N. G., Mahowald, N. M., Soreghan, G. S., Soreghan, M. J., & Shields, C. A. (2015). A model-based evaluation of tropical climate in pangaea during the late palaeozoic icehouse. *Palaeogeography, Palaeoclimatology, Palaeoecology*, *425*, 109-127. Retrieved from https://www.sciencedirect.com/science/article/pii/S0031018215000802 doi: https://doi.org/10.1016/j.palaeo.2015.02.024

Horton, D. E., Poulsen, C. J., Montañez, I. P., & DiMichele, W. A. (2012). Eccentricity-paced late Paleozoic climate change. *Palaeogeography, Palaeoclimatology, Palaeoecology*, *331-332*, 150-161. Retrieved from https://www.sciencedirect.com/science/article/pii/S003101821200154X doi: https://doi.org/10.1016/j.palaeo.2012.03.014

Hyde, W. T., Crowley, T. J., Baum, S. K., & Peltier, W. R. (2000, May). Neoproterozoic 'snowball Earth' simulations with a coupled climate/ice-sheet model. *Nature*, *405*(6785), 425–429. doi: 10.1038/35013005

Julien, A. (1895). Ancien glaciers de la période houillère dans le plateau central de la France. *Ann. Club Alp. Fr.*, *21*, 1–28.

Kaser, G. (1999). A review of the modern fluctuations of tropical glaciers. *Global and Planetary Change*, *22*(1), 93-103. Retrieved from https://www.sciencedirect.com/science/article/pii/S0921818199000284 doi: https://doi.org/10.1016/S0921-8181(99)00028-4

Kotlarski, S., Jacob, D., Podzun, R., & Paul, F. (2010, Jan). Representing glaciers in a regional climate model. *Climate Dynamics*, *34*(1), 27–46. doi: 10.1007/s00382-009-0685-6

La Frenierre, J., & Mark, B. G. (2017). Detecting Patterns of Climate Change at Volcán Chimborazo, Ecuador, by Integrating Instrumental Data, Public Observations, and Glacier Change Analysis. *Annals of the American Association of Geographers*, *107*(4), 979-997. Retrieved from `https://doi.org/10.1080/24694452.2016.1270185` doi: 10.1080/24694452.2016.1270185

Larsen, I. J., Montgomery, D. R., & Greenberg, H. M. (2014, 06). The contribution of mountains to global denudation. *Geology*, *42*(6), 527-530. Retrieved from `https://doi.org/10.1130/G35136.1` doi: 10.1130/G35136.1

Lawrence, D. M., Fisher, R. A., Koven, C. D., Oleson, K. W., Swenson, S. C., Bonan, G., ... Zeng, X. (2019). The Community Land Model Version 5: Description of New Features, Benchmarking, and Impact of Forcing Uncertainty. *Journal of Advances in Modeling Earth Systems*, *11*(12), 4245-4287. Retrieved from `https://agupubs.onlinelibrary.wiley.com/doi/abs/10.1029/2018MS001583` doi: https://doi.org/10.1029/2018MS001583

Lipscomb, W. H., Price, S. F., Hoffman, M. J., Leguy, G. R., Bennett, A. R., Bradley, S. L., ... Worley, P. H. (2019). Description and evaluation of the community ice sheet model (cism) v2.1. *Geoscientific Model Development*, *12*(1), 387–424. Retrieved from `https://gmd.copernicus.org/articles/12/387/2019/` doi: 10.5194/gmd-12-387-2019

Loomis, S. E., Russell, J. M., Verschuren, D., Morrill, C., De Cort, G., Sinninghe Damsté, J. S., ... Kelly, M. A. (2017). The tropical lapse rate steepened during the Last Glacial Maximum. *Science Advances*, *3*(1). Retrieved from `https://advances.sciencemag.org/content/3/1/e1600815` doi: 10.1126/sciadv.1600815

Mills, B. J., Donnadieu, Y., & Goddéris, Y. (2021). Spatial continuous integration of Phanerozoic global biogeochemistry and climate. *Gondwana Research*. Retrieved from `https://www.sciencedirect.com/science/article/pii/S1342937X21000721` doi: https://doi.org/10.1016/j.gr.2021.02.011

Minder, J. R., Mote, P. W., & Lundquist, J. D. (2010). Surface temperature lapse rates over complex terrain: Lessons from the Cascade Mountains. *Journal of Geophysical Research: Atmospheres*, *115*(D14). Retrieved from `https://agupubs.onlinelibrary.wiley.com/doi/abs/10.1029/2009JD013493` doi: https://doi.org/10.1029/2009JD013493

Mölg, T., Hardy, D. R., Cullen, N. J., & Kaser, G. (2008). Tropical Glaciers, Climate Change, and Society: focus on Kilimanjaro (East Africa). In *Darkening peaks: glacier retreat, science, and society.* Berkeley: University of California Press.

Mölg, T., & Kaser, G. (2011). A new approach to resolving climate-cryosphere relations: Downscaling climate dynamics to glacier-scale mass and energy balance without statistical scale linking. *Journal of Geophysical Research: Atmospheres*, *116*(D16). Retrieved from `https://agupubs.onlinelibrary.wiley.com/doi/abs/10.1029/2011JD015669` doi: https://doi.org/10.1029/2011JD015669

Mote, P., & Kaser, G. (2007). The Shrinking Glaciers of Kilimanjaro: Can Global Warming Be Blamed? *American Scientist*, *95*(4), 318. doi: 10.1511/2007.66.318

NCAR. (2018). *b.e21.BHIST.f09_g17.CMIP6-historical.003 data.* Earth System Grid. Retrieved from `https://www.earthsystemgrid.org/dataset/ucar.cgd.cesm2.b.e21.BHIST.f09_g17.CMIP6-historical.003.html`

Osmaston, H. (2004). Quaternary glaciation in the East African mountains. In *Quaternary Glaciations - Extent and Chronology Part III: South America, Asia, Africa, Australia, Antarctica.* Amsterdam: Elsevier.

Pepin, N. C., Maeda, E. E., & Williams, R. (2016). Use of remotely sensed land surface temperature as a proxy for air temperatures at high elevations: Findings from a 5000 m elevational transect across Kilimanjaro. *Journal of Geophysical Research: Atmospheres*, *121*(17), 9998-10,015. Retrieved from `https://agupubs.onlinelibrary.wiley.com/doi/abs/10.1002/2016JD025497` doi:

https://doi.org/10.1002/2016JD025497

Pfeifer, L. S., Soreghan, G. S., Pochat, S., & Van Den Driessche, J. (2021, Jan). Loess in eastern equatorial pangea archives a dusty atmosphere and possible upland glaciation. *GSA Bulletin*, *133*(1–2), 379–392. doi: 10.1130/B35590.1

Porter, S. C. (2001). Snowline depression in the tropics during the last glaciation. *Quaternary Science Reviews*, *20*(10), 1067-1091. Retrieved from `https://www.sciencedirect.com/science/article/pii/S0277379100001785` doi: https://doi.org/10.1016/S0277-3791(00)00178-5

Poulsen, C. J., Pollard, D., Montañez, I. P., & Rowley, D. (2007). Late Paleozoic tropical climate response to Gondwanan deglaciation. *Geology*, *35*(9), 771. doi: 10.1130/G23841A.1

Roe, G. H., Christian, J. E., & Marzeion, B. (2021). On the attribution of industrial-era glacier mass loss to anthropogenic climate change. *The Cryosphere*, *15*(4), 1889–1905. Retrieved from `https://tc.copernicus.org/articles/15/1889/2021/` doi: 10.5194/tc-15-1889-2021

Shannon, S., Smith, R., Wiltshire, A., Payne, T., Huss, M., Betts, R., … Harrison, S. (2019). Global glacier volume projections under high-end climate change scenarios. *The Cryosphere*, *13*(1), 325–350. Retrieved from `https://tc.copernicus.org/articles/13/325/2019/` doi: 10.5194/tc-13-325-2019

Shen, Y.-J., Shen, Y., Goetz, J., & Brenning, A. (2016). Spatial-temporal variation of near-surface temperature lapse rates over the Tianshan Mountains, central Asia. *Journal of Geophysical Research: Atmospheres*, *121*(23), 14,006-14,017. Retrieved from `https://agupubs.onlinelibrary.wiley.com/doi/abs/10.1002/2016JD025711` doi: https://doi.org/10.1002/2016JD025711

Soreghan, G. S., Soreghan, M. J., Poulsen, C. J., Young, R. A., Eble, C. F., Sweet, D. E., & Davogustto, O. C. (2008). Anomalous cold in the Pangaean tropics. *Geology*, *36*(8), 659. doi: 10.1130/G24822A.1

Soreghan, G. S., Sweet, D. E., & Heavens, N. G. (2014). Upland glaciation in tropical pangaea: Geologic evidence and implications for late paleozoic climate modeling. *The Journal of Geology*, *122*(2), 137-163. Retrieved from `https://doi.org/10.1086/675255` doi: 10.1086/675255

Thompson, L. G., Mosley-Thompson, E., Davis, M. E., & Brecher, H. H. (2011). Tropical glaciers, recorders and indicators of climate change, are disappearing globally. *Annals of Glaciology*, *52*(59), 23–34. doi: 10.3189/172756411799096231

Tripati, A. K., Sahany, S., Pittman, D., Eagle, R. A., Neelin, J. D., Mitchell, J. L., & Beaufort, L. (2014, Mar). Modern and glacial tropical snowlines controlled by sea surface temperature and atmospheric mixing. *Nature Geoscience*, *7*(3), 205–209. doi: 10.1038/ngeo2082

UCAR. (n.d.). *2. CLM Technical Note — ctsm release-clm5.0 documentation.* Retrieved from `https://escomp.github.io/ctsm-docs/versions/release-clm5.0/html/tech_note/index.html`

Van Tricht, K., Lhermitte, S., Gorodetskaya, I. V., & van Lipzig, N. P. M. (2016). Improving satellite-retrieved surface radiative fluxes in polar regions using a smart sampling approach. *The Cryosphere*, *10*(5), 2379–2397. Retrieved from `https://tc.copernicus.org/articles/10/2379/2016/` doi: 10.5194/tc-10-2379-2016

Vizcaíno, M., Lipscomb, W. H., Sacks, W. J., & van den Broeke, M. (2014). Greenland Surface Mass Balance as Simulated by the Community Earth System Model. Part II: Twenty-First-Century Changes. *Journal of Climate*, *27*(1), 215 - 226. Retrieved from `https://journals.ametsoc.org/view/journals/clim/27/1/jcli-d-12-00588.1.xml` doi: 10.1175/JCLI-D-12-00588.1

Vuille, M., Francou, B., Wagnon, P., Juen, I., Kaser, G., Mark, B. G., & Bradley, R. S. (2008). Climate change and tropical Andean glaciers: Past, present and future. *Earth-Science Reviews*, *89*(3), 79-96. Retrieved from `https://`

www.sciencedirect.com/science/article/pii/S0012825208000408 doi: https://doi.org/10.1016/j.earscirev.2008.04.002

Wagnon, P., Lafaysse, M., Lejeune, Y., Maisincho, L., Rojas, M., & Chazarin, J. P. (2009). Understanding and modeling the physical processes that govern the melting of snow cover in a tropical mountain environment in Ecuador. *Journal of Geophysical Research: Atmospheres*, *114*(D19). Retrieved from https://agupubs.onlinelibrary.wiley.com/doi/abs/10.1029/2009JD012292 doi: https://doi.org/10.1029/2009JD012292

WMO. (1957). Meteorology — a three dimensional science: Second session of the commission for aerology. *WMO Bulletin*, *4*(4), 134–138.

Figure 1.

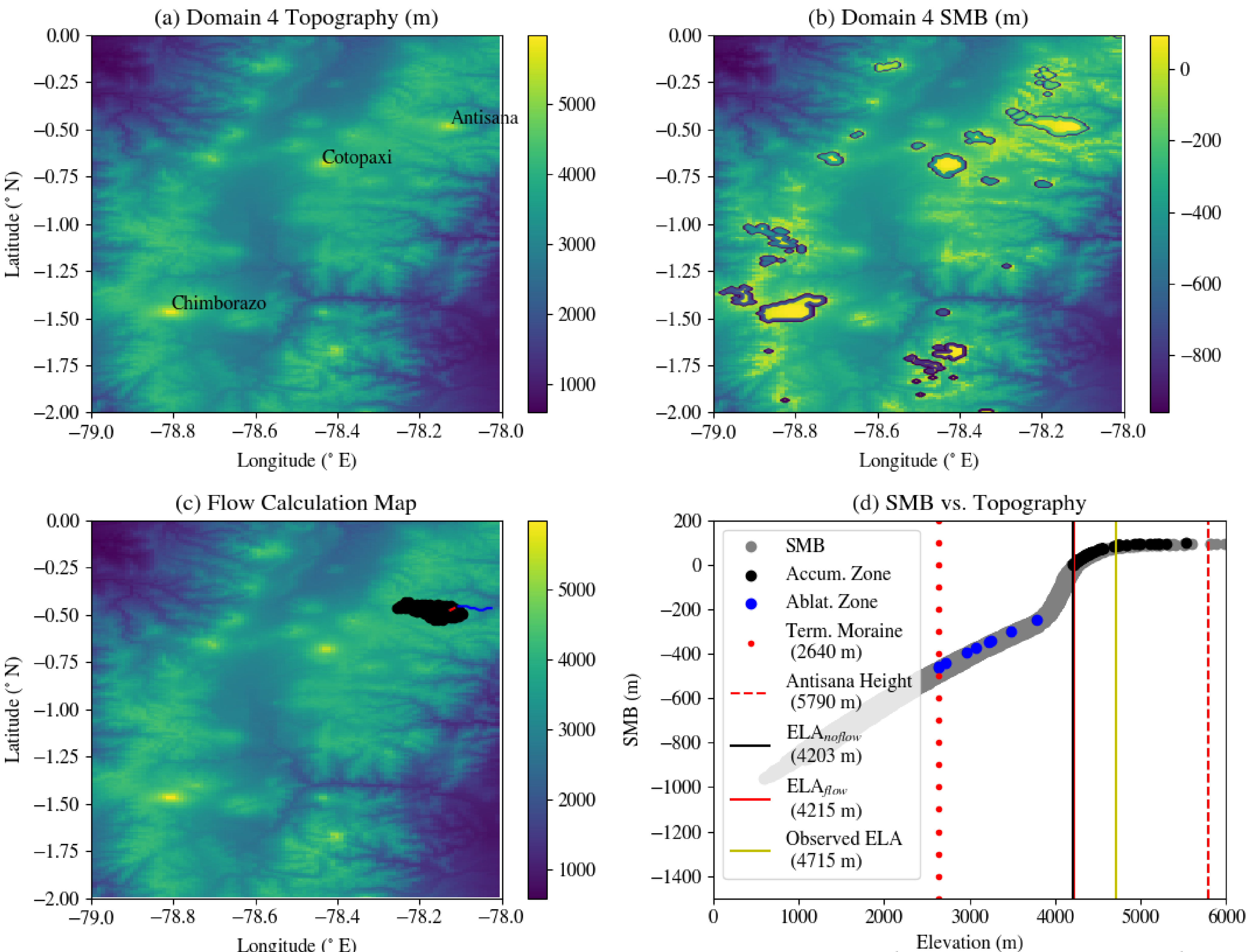

(a) Domain 4 Topography (m)
Antisana
Cotopaxi
Chimborazo
Latitude (° N)
Longitude (° E)
(b) Domain 4 SMB (m)
Latitude (° N)
Longitude (° E)
(c) Flow Calculation Map
Latitude (° N)
Longitude (° E)
(d) SMB vs. Topography
SMB
Accum. Zone
Ablat. Zone
Term. Moraine (2640 m)
Antisana Height (5790 m)
ELA_{noflow} (4203 m)
ELA_{flow} (4215 m)
Observed ELA (4715 m)
SMB (m)
Elevation (m)
Simulation Lapse Rate = 7 K km^{-1} \ Free Air Lapse Rate=6.56 K km^{-1}

Figure 2.

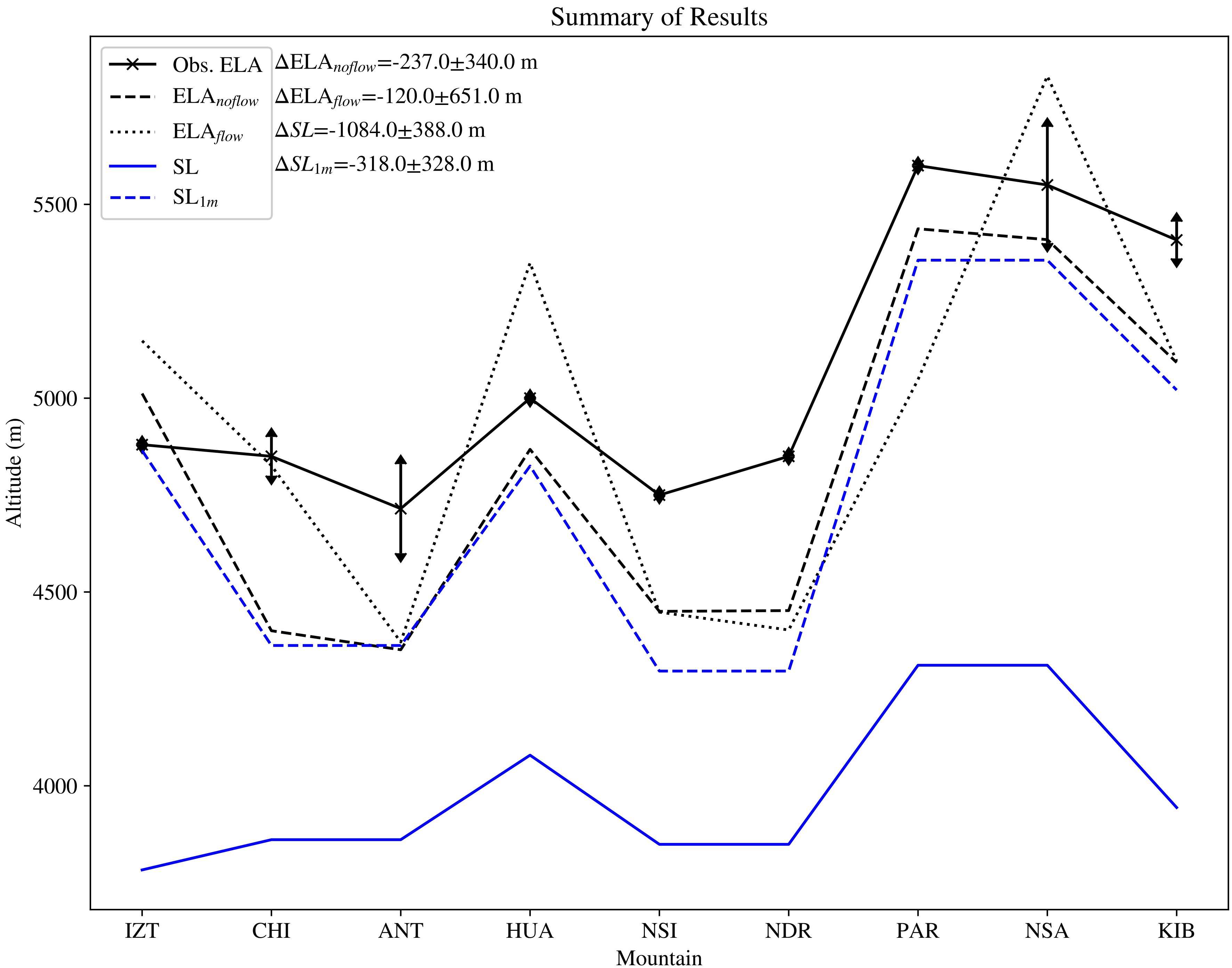

Summary of Results
Obs. ELA
ELA_{noflow}
ELA_{flow}
SL
SL_{1m}
ΔELA_{noflow}=-237.0±340.0 m
ΔELA_{flow}=-120.0±651.0 m
ΔSL=-1084.0±388.0 m
ΔSL_{1m}=-318.0±328.0 m
5500
5000
4500
4000
Altitude (m)
IZT
CHI
ANT
HUA
NSI
NDR
PAR
NSA
KIB
Mountain